Laboratory modelling of vertical sediment mixing in the surf zone

Takayuki Suzuki [a*], Kiichi Tajima [b] and Ravindra Jayaratne [c]

[a*] Department of Civil Engineering, Yokohama National University, Tokiwadai 79-5, Hodogaya, Yokohama, Kanagawa, 240-8501, Japan
suzuki-t@ynu.ac.jp

[b] Metropolitan Expressway Company Limited
1-4-1 Kasumigaseki, Chiyoda-ku, Tokyo, Japan
shirokumabado@gmail.com

[c] Department of Engineering & Construction, School of Architecture, Computing & Engineering, University of East London, Docklands Campus, 4-6 University Way, London E16 2RD, UK
r.jayaratne@uel.ac.uk

Laboratory modelling of vertical sediment mixing in the surf zone

Abstract

A comprehensive set of laboratory experiments were conducted to investigate the spatial distributions of mixing depth in the surf zone. A wooden sandbox of 0.15-m-deep and 1.0-m-long is fabricated and placed in the middle of the bed slope. In the experiments, five different sediment diameters, 0.32, 0.77, 1.14, 2.0 and 2.85 mm, were used and the same diameters of fluorescent sand tracers were sprinkled on the sand bed surface to investigate the mixing depth. After a specific duration of regular wave generation, wave height, H = 8.4 cm and wave period, T = 1.5 s, core samples were taken at six different cross-shore locations in the surf zone and analyzed the mixing depth. Moreover, the flow velocity field in the surf zone was obtained by using a Large Eddy Simulation (LES) model and discussed the relationship with spatial distributions of mixing depth. The results reveal that the mixing depth has cross-shore spatial variation and the maximum mixing depth occurred at the impinging point for all tested sediment diameters. The spatial distributions for each diameter were repeatable, however the depth decreases in a logarithmic manner from smaller to larger grain size. Furthermore, the spatial distribution of mixing depth is correlated with the bottom Root Mean Square (RMS) vertical velocity and proposed a new simple mathematical relationship for mixing depth which shows good accuracy with experimental data.

Keywords: mixing depth, fluorescent sand tracer, spatial distribution, laboratory experiment, Large Eddy Simulation

1. Introduction

In the nearshore region, active sediment transport occurs due to wave and current actions and evolves in beach profile changes. A significant amount of sediment suspension occurs in the surf zone and hence a dramatic change to the morphology, especially during stormy wave conditions. Due to the wave action, not only sediment suspension/movement but also sediment vertical mixing occurs in the surf zone. Understanding of the bed surface sediment mixing process is vital as it supports our knowledge on proper construction of coastal structures, implementation of beach nourishment programs etc. (e.g., Fucella and Dolan, 1996), eco system studies (e.g., Botton et al., 1988) and sediment pollution studies (e.g., Owens and Lee, 2003).

Greater knowledge of sediment mixing processes is of paramount importance not only for engineering design aspects such as coastal zone management, but also for ecological aspects, e.g., marine plants and animals. Therefore, nearshore-sediment mixing has been analyzed via the sediment mixing depths obtained. There are three widely used field methods for the determination of the sand mixing depth, hence the definition of mixing is given accordingly (Ciavola et al., 1997a): the first method consists of digging a hole and filling it up to the surface level with colored sand (e.g., King, 1951; Williams, 1971; Ciavola et al., 1997b), the second method is identified with the usage of depth of disturbance rods and washes (e.g., Greenwood and Hale, 1980). The third method assesses the distribution in cores of a known quantity of sand tracers injected: this gives the depth of mixing (e.g., Kraus, 1985; Ciavola et al., 1997b). The present study follows the third field method explained above hence the methodology and definition is as follows. The authors conducted the core sampling before the experiment has started to find the infiltrated depth of fluorescent sand for each tested

sediment diameter, i.e., the minimum quantity of fluorescent sand tracers without mixing. Once the core sampling analysis was performed after the experiment, if the number of fluorescent sand tracers are greater than the minimum quantity of tracers, this particular depth was defined as the mixing depth. The definition of the mixing depth is further described in the 2.1.2 Core sampling section.

King (1951) investigated vertical sediment mixing through a series of field measurements. Some researchers started to explore the correlation of vertical sediment mixing with wave height and breaking processes (e.g., Williams, 1971; Gaughan, 1978). On estimating the depth of sediment mixing, Sunamura and Kraus (1984) measured vertical mixing at several coasts in Japan and reported that the average mixing depth in the surf zone would be 2.7% of the wave breaker height. Sherman et al. (1994) conducted field measurements at a low energy reflected beach in the USA and found that mixing depth is 22% of the significant wave height (H_s). Ciavola et al. (1997a) also conducted field measurements and found that the averaged mixing depth is proportional to the wave period (T) and reported that the averaged mixing depth was 27% of the wave breaker height.

While the mixing depth was affected by several wave hydrodynamic parameters that were different depending on the characteristics of each coast, Sherman et al. (1993) discussed the mixing depth associated with mega ripples and showed that the depth was about four times larger than the wave height (H). Moreover, the mixing depth at different beach conditions has been investigated. Dolphin et al. (1995) conducted field observations at an intertidal sand flat in an enclosed sea in New Zealand. Anfuso et al. (2000) reported the characteristics of mixing depth at the reflected, barred dissipative, and dissipative beaches in Spain. Vila-Concejo et al. (2014) investigated the depth on a

coral reef environment in Australia and showed that mixing depth was small, yet they were large values predicted by the empirical formulae for gentle siliciclastic beaches. Moreover, the effects of bed slope (e.g., Jackson and Nordstrom, 1993; Ferreira, 2000), wave type (e.g., Aagaard and Jensen, 2013), sediment diameter difference (e.g., Saini et al., 2009), etc. have been investigated. Table 1 summarizes some of the key empirical relationships of sediment mixing depths.

Table 1. Published empirical relationships for sediment mixing depth in surf zone.

Source	Empirical relationship [m]	H_s [m]	T [s]	Beach slope [$tan\beta$]
Greenwood and Hale (1980)	$z_m = 0.35$	$H_b = 2.0$	6.5	-
Sunamura and Kraus (1984)	$z_m = 0.027\ H_b$	0.60 - 1.11	4.9 - 10.2	0.6 - 5.7
Katoh and Tanaka (1986)	$z_m = 0.05\ H_b$	0.38 - 0.80	5.1 - 7.0	-
Sherman et al. (1994)	$z_m = 0.22\ H_b$	1.22	-	-
Ciavola et al. (1997a)	$z_m = 0.27\ H_b$	0.34 - 0.80	5.1 - 7.0	5.70 - 7.90
Ferreira et al. (2000)	$z_m = 0.23\ H_b$ $z_m = 1.86\ H_{bs}\ tan\beta$	0.92	8.0	0.08
Jackson and Malvarez (2002)	$z_m = 0.24\ H_b$	2.00 - 3.00	8.5	-
Saini et al. (2009)	$z_m = 0.22\ H_b$	0.40	9.0	-
Belliod et al. (2011)	$z_m = 0.029\ H_{bs}\ tan\beta$	0.16 - 0.20	7.0 - 9.0	0.08

* z_m: sediment mixing depth, H_s: significant wave height, H_b: wave breaker height, T:

wave period.

Many mixing depth equations developed so far were proportional to wave breaker height. However, the coefficient of the wave breaking height shows a large difference depending on the location of the coast, and these equations could only show the averaged mixing depth in the surf zone. Although the sediment mixing occurred not only by the wave action but also due to benthos communities (e.g., Kraeuter and Fegley, 1994), in this research study, the spatial distribution of mixing depth in the surf zone that is affected by the hydrodynamic processes is the focus. A series of comprehensive laboratory experiments were conducted in a state-of-the-art small-scale physical modelling facility, and the sediment mixing against several sediment diameters in the surf zone were investigated in detail.

2. Methodology

2.1 Laboratory experiments

2.1.1 Flume setup and wave condition

The flume experiments were conducted in a side-wall-glass flume with dimensions of 0.6 × 0.6 × 17 m at Yokohama National University (YNU). Figure 1 shows a schematic sketch of the wave flume and arrangement of measuring equipment. A wooden sandbox of 0.15-m-deep and 1.0-m-long is fabricated, and the box is placed in the middle of the bed slope of 1:10. The slope was made using impermeable aluminum sheets. The cross-shore direction is set as x-axis and the origin is set at the offshore end of the sand box.

In the experiments, five different sediment diameters, i.e., d_{50} = 0.32, 0.77, 1.14, 2.0 and 2.85 mm were used to cover typical sand to coarse grain sand. For each test run,

123 sand that filled on the slope was replaced with the different sediment diameter. In the
124 sandbox section, three capacitance type wave gauges (CH-704, KENEK) were fixed at x
125 = 0, 45.0 and 84.0 cm to measure the incident wave heights. Prior to the experiments,
126 the water depth, h was set at 33.0 cm, and several regular wave conditions were tested
127 to determine the wave heights and wave periods for different breaker types, i.e., spilling
128 to plunging range, covering the wave impingement points within the sandbox area.
129 Based on the preliminary test runs, a wave height of 8.4 cm and period of 1.5 s
130 measured at x = -940 cm (W_1 in Figure 1) was selected for these experiments. In the
131 wave flume, wave breaking point and wave impingement points were identified at x = -
132 65 and 60 cm, respectively. The duration of each test run was set to 3 minutes. Figure 2
133 shows an experimental photograph taken from the side of the wave flume, showing an
134 overview of a wave breaking from left to right.
135 On sediment transport, that leads to change the beach profile, measured coastal
136 parameters such as the Eulerian velocity and suspended sediment concentration are
137 sensible to use for the analysis. However, the Lagrangian observation of sand movement
138 is also required for the detailed understanding of sediment motion. For this purpose,
139 fluorescent sand tracers have been used in field measurements and laboratory
140 experiments (e.g., Kraus and Smith, 1994; Silva et al., 2007; Suzuki et al., 2019). Thus,
141 authors also used the fluorescent sand in the present set of laboratory experiments.
142 At the beginning of each test run, fluorescent sand tracers were spread evenly
143 on the top of the sand bed. It was noted that each diameter of fluorescent sand tracers,
144 except d_{50} = 0.32 mm, was generated by hand using fluorescent spray, and the same
145 diameter of the tracers of 240 g was used for each test run. Regarding the colored
146 fluorescent sand, we carefully sprayed the fluorescent liquid on the sediment and mixed

it with un-colored sand to create a thin coating. Therefore, we considered the grain size of colored sand to be approximately the same as non-colored sand.

After each experiment, core sample was taken, and the bed profile was surveyed over the sandbox area using a sand surface measuring instrument (WH-601, KENEK Co.). The sand bed profile was measured every 5.0 cm internally along the middle of the flume.

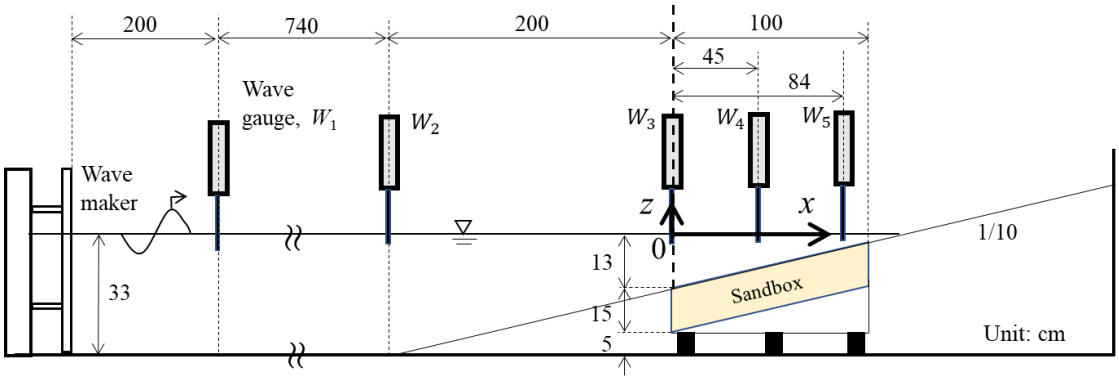

Figure 1. Experimental setup of the 2D wave flume and measuring equipment.

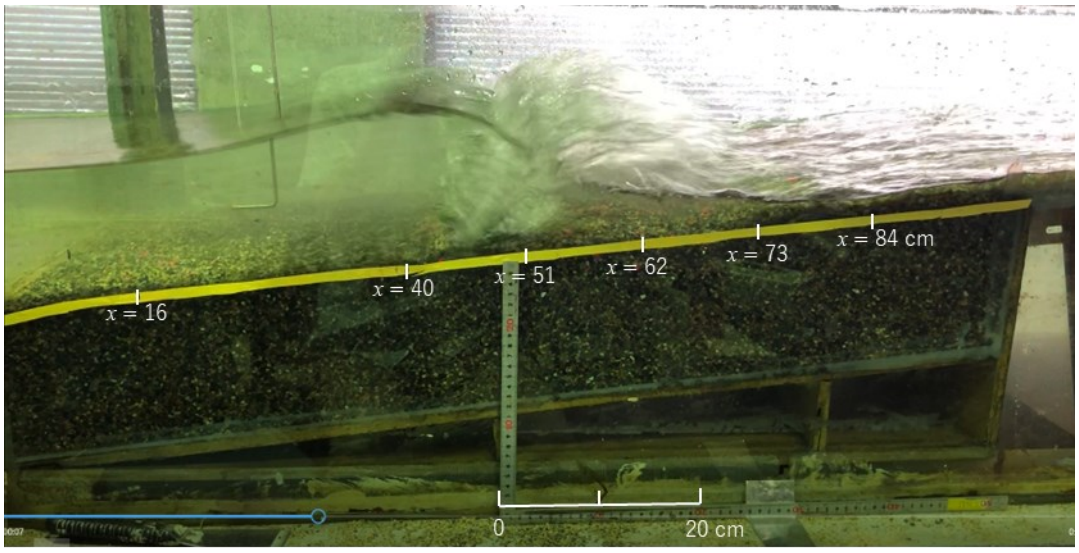

Figure 2. A laboratory photograph taken from the side of the wave flume, showing an

159 overview of a wave breaking from left to right.

160

161 *2.1.2 Core sampling*

162 After each trial run, six core samples were collected from the sand bed with an
163 equidistant separation of 11 cm except the offshore side of two cores, i.e., 24 cm, as
164 shown in Figure 3. A PVC tube with a length of 20 cm and a diameter of 2.6 cm was
165 used for the sampling. After removing the sand core, the bottom of the tube was sealed.
166 These tubes were then pushed gently by a plastic stick with the same inner diameter of
167 the tube from the top, and the cores were sub divided into 5-mm thick layers. The 5-mm
168 thick layered samples were air-dried for several days and taken to a dark room to count
169 the number of fluorescent sand tracers manually in each layer using an UV light.

170

171

172 Figure 3. Locations of the core samples taken in the surf zone.

173

174

175 Before conducting the experiments, the authors checked how many fluorescent

sand tracers were infiltrated into the core sampler without sediment mixing process. Figure 4 shows fluorescent sand tracer counted from each depth for five sediment diameters. Even without mixing, some particles were found at several depths within the core. Therefore, for each sediment diameter, the authors decided the minimum quantity of fluorescent sand tracer to be 4, 3, 3, 1, 1 for the sand diameters 0.32, 0.77, 1.14, 2.0, 2.85 mm, respectively. Thus, in this analysis, when the number of fluorescent sand tracers are greater than the above-mentioned value from the 5-mm thick sample, that depth is taken as the mixing depth of the entire core sample. If the tracers found in the sample were less than the minimum threshold value, it is considered that the sediment mixing has not occurred at that depth. Moreover, since 0.5 cm vertical mixing occurred in all test cases, the analyzed results will include 0.5 cm uncertainty depth.

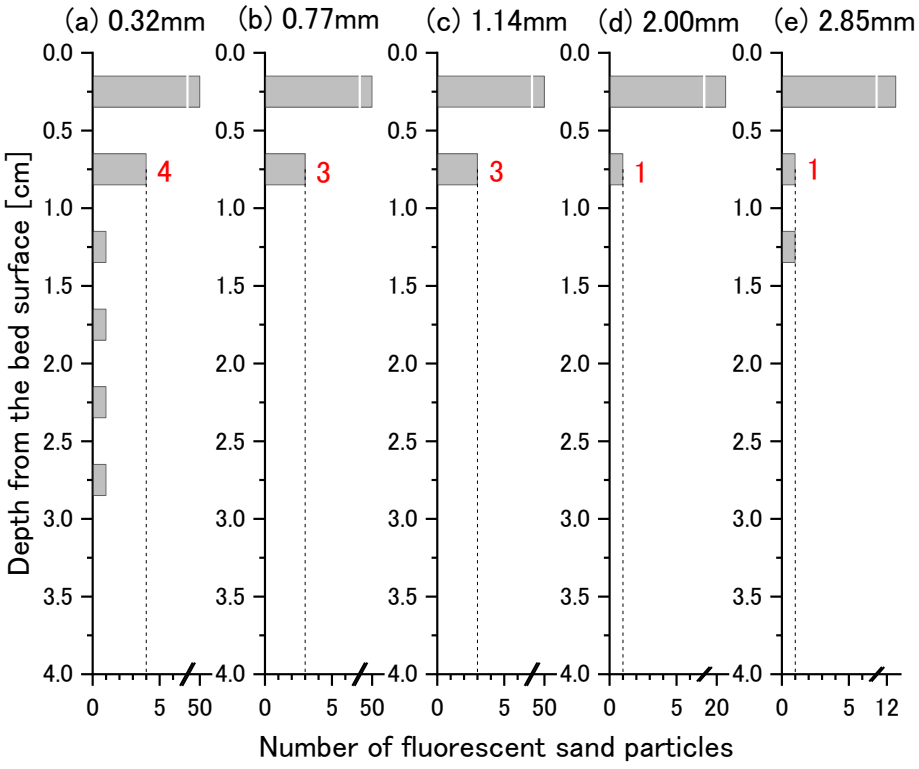

189 Figure 4. Number of fluorescent sand tracers at each depth for five sediment diameters
190 without vertical sediment mixing, by manual counting. Dashed lines indicate the lower
191 criteria for each sediment diameter.

192 A 60 cm wide wave flume was used in this experiment. Since the main focus
193 area of this study is the surf zone, sediment mixing is considered to be three-
194 dimensional. However, by setting the duration of the experiment to 3 minutes, the
195 distribution of mixing depth in the longshore direction is considered to be almost
196 uniform. Regarding the repeatability of the experiment of the mixing depth, the authors
197 thoroughly checked the mixing depth of 1.15 mm sediment at the same cross-shore
198 location but at a different longshore location. The mixing depths are summarized in
199 Table 2. Every experimental step in each test run was performed in a highly controlled
200 manner, and observational errors due to measurements (mixing depth) were considered
201 to be small.

202

203 Table 2. Repeatability of mixing depth in the same wave and sediment conditions.

204

Cross-shore location, x [cm]	Mixing depth [mm]	
	1st	2nd
16	0	0
40	30	30
51	20	20
62	20	25
73	15	15
84	15	20

205

206

207 ***2.2 Numerical simulation***

Until now, several numerical models have been proposed, and accurate estimations of velocity fields have been reported (e.g., Christensen and Deigaard, 2001; Roselli et al., 2019). Moreover, sediment suspension and mixing in the surf zone by breaking waves have been simulated before (e.g., Zou and Dalrymple, 2006; Suzuki et al., 2007; Zhou et al., 2017). In this study, the authors used a Large Eddy Simulation (LES) model to calculate the velocity field in the surf zone.

2.2.1 Outline of the Large Eddy Simulation (LES) model

A single-phase (liquid-phase) Large Eddy Simulation (LES) model is used to calculate the fluid velocities under the experimental wave conditions. The LES approach is applicable for higher Reynolds turbulence flows, which separate the small and large-scale eddies. The Reynolds-averaged Navier-Stokes equation (Eq. 1) and continuity equation (Eq. 2) are used to solve the generated large eddies, whereas the small eddies are solved using a turbulence model by a sub-grid scale (SGS) approach.

$$\frac{\partial \overline{u_i}}{\partial t} + \overline{u_j}\frac{\partial \overline{u_i}}{\partial x_j} = -\frac{1}{\rho}\frac{\partial \overline{p}}{\partial x_i} + \nu\frac{\partial^2 \overline{u_i}}{\partial x_j{}^2} - \frac{\partial}{\partial x_j}\left(\tau_{ij}\right) + g_i \quad (1)$$

$$\frac{\partial \overline{u_i}}{\partial x_i} = 0 \quad (2)$$

where $\overline{u_i}$ is the spatially averaged velocity over the grid size, t is the time, x_i (i = 1, 2, and 3) are the x, y and z coordinate components, ρ is the density of the fluid, p is the pressure, ν is the molecular viscosity, g is the gravitational acceleration, and τ_{ij} is the sub-grid scale (SGS) stress, which is estimated by the Smagorinsky model (Smagorinsky, 1963). The free-surface position is calculated using the density function

230 method based on the work of Watanabe and Saeki (1999). Thus, density function $f \geq 0.5$
231 indicates a water cell and $f < 0.5$ indicates an air cell. The water surface is assumed to be
232 located on a curve where the density function is equal to 0.5.
233 A three-dimensional cartesian coordinate system was used to define the model
234 domain. Computational grids containing 600 cells in the x direction, 24 in the y-
235 direction, and 52 in the z-direction were adopted with a grid length of 1 cm with the
236 origin at the offshore edge of the bottom slope, x = -200 cm (Figure 1), and the domain
237 was sloped as 1/10. The calculation was started from the still-water condition, and the
238 computational time step (Δt) was set as 0.00064 s. This time step was determined
239 iteratively until computational stability was achieved. For the numerical calculations, a
240 duration of 26 s was simulated with input values of the wave height (H), period (T) and
241 depth (h), which were as same as in the laboratory experiments. The simulation results
242 of the water surface elevations, wave heights, water flow velocities along the sand bed
243 region were used for the analysis. Note that the LES model did not calculate the beach
244 profile change.
245
246 2.2.2 Model verification
247 The calculated water surface elevations were verified by the measured wave heights in
248 the experiments. The calculated and measured water elevations at x = -200 cm (edge of
249 the bottom slope), 45 cm and 84 cm were shown in Figure 5. The LES model seems to
250 slightly underestimate wave heights compared to the experimental values. However, the
251 calculated values exhibit an overall agreement with the experiments with a correlation
252 coefficient of R = 0.90 (x = 45 cm) and R = 0.69 (x = 84 cm).
253 For the velocity verification, Gunaratna et al. (2018) carried out experiments

using the same wave flume at YNU with similar wave conditions. The velocity fields of 15.0×15.0 cm^2 were recorded by a high-speed camera (KIII, Kato Koken Co. Ltd.) with a capture rate of 100 fps. The numerical and experimental cross-shore velocity magnitudes with different phases were compared, and the overall vertical profiles and magnitudes exhibit good agreement (R = 0.69). It can be concluded that LES model gives consistent and accurate results to compare the experimental sediment mixing tests.

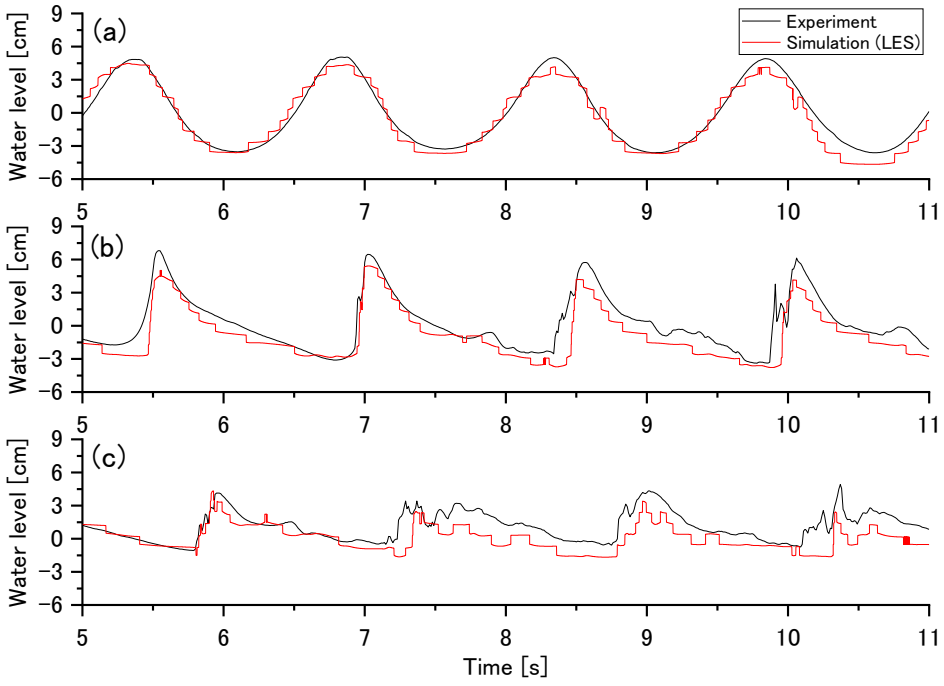

Figure 5. Numerical and experimental results of the surface elevation, (a) x = 0 cm, (b) x = 45 cm and (c) x = 84 cm.

3. Experimental and Numerical Results

3.1 Bed profile change

Five sediment diameters were used in the laboratory experiments. After making regular

waves of 3-minute duration, the bed profile change was measured by a sand-bed profiler (WHT-60, KENEK), and core sampling was conducted at six different locations. Figure 6 shows the bed profile change for all experimental cases. At the impingement point, x = 62 cm, the profile of case 1 (d_{50} = 0.32 mm) shows considerable erosion. However, for the other cases, erosion occurred further onshore, i.e., around x = 73 cm. As the sediment diameter increases from 0.32 to 2.85 mm, the sediment tends to move offshore-ward while the profile change decreases.

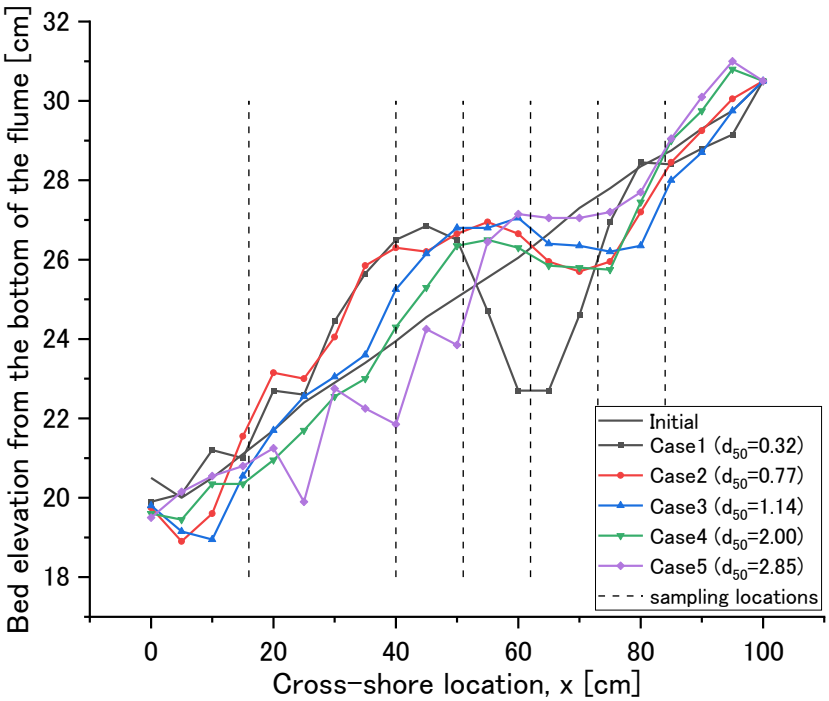

Figure 6. Bed profile change for different sediment diameters. Vertical dotted lines indicate the core sampling locations.

3.2 Spatial distributions of mixing depth

The core samplings were conducted at the six cross-shore locations along the sandbox (vertical dashed lines in Figure 6). Figure 7 shows the core sampling results of case 1 (d_{50} = 0.32 mm) for each sampling location. The x-axis represents the number of fluorescent sand particles whereas the y-axis shows the depth from the initial bed level at each location. The horizontal dashed and solid lines indicate the bed level of before (initial) and after the experiment, respectively. The negative depth value indicates the deposition. Masked areas were neglected from the analysis because of the lower number of fluorescent sand tracers.

The results show that the deposition occurred between x = 40 and 51 cm, and erosion occurred between x = 62 and 73 cm. The profile change was small at onshore and offshore ends, i.e., x = 16 and 84 cm. At the locations of sediment deposition, the mixing depth is considered as the depth from the initial bed level. For all the sampling locations, more than 2 cm of sediment mixing was observed, and the maximum mixing depth was at the impingement point and has become a lower value for both nearshore and offshore regions.

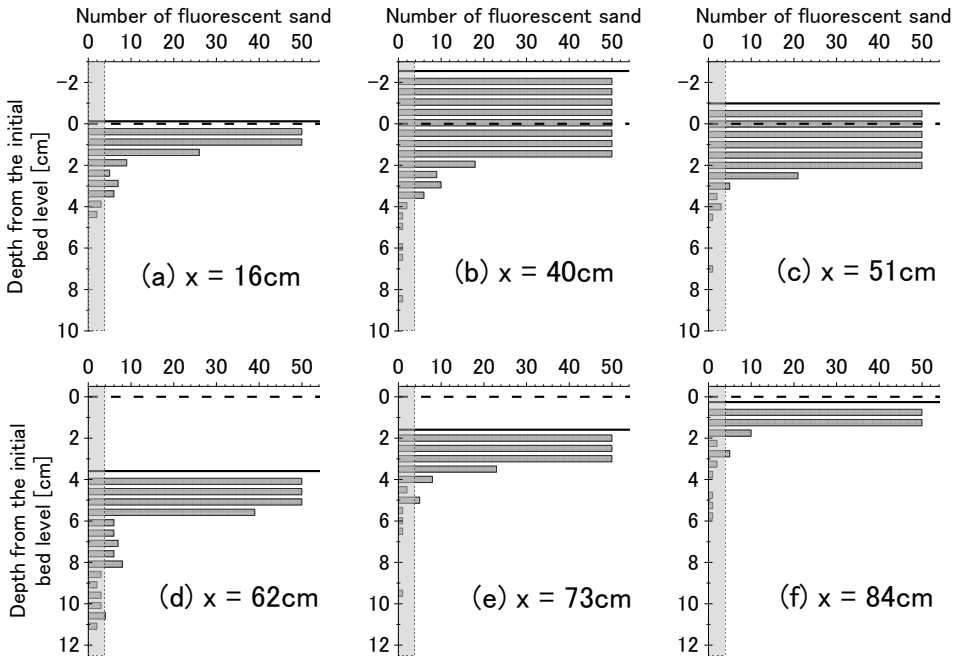

Figure 7. Core sampling results of case 1 (d_{50} = 0.32 mm) for each location, (a) x = 16 cm, (b) x = 40 cm, (c) x = 51 cm, (d) x = 62 cm, (e) x = 73 cm, and (f) x = 84 cm. Horizontal dashed and solid lines indicate the bed level before and after the experiment, respectively. The lower than the lowest criteria of number of fluorescent sand tracers are shown as a mask and neglected in the analysis.

Figure 8 shows the spatial distributions of mixing depth for all cases, and each value is summarized in Table 3. The maximum mixing occurred at the impinging point, x = 62 cm, for all test cases, and larger mixing depth occurred for the smaller sediment diameter. The averaged mixing depth for d_{50} = 0.32 mm is approximately 3.39 cm and decreased logarithmically up to 0.58 cm for d_{50} = 2.85 mm. Spatial distributions were similar for all test cases except at x = 51 cm.

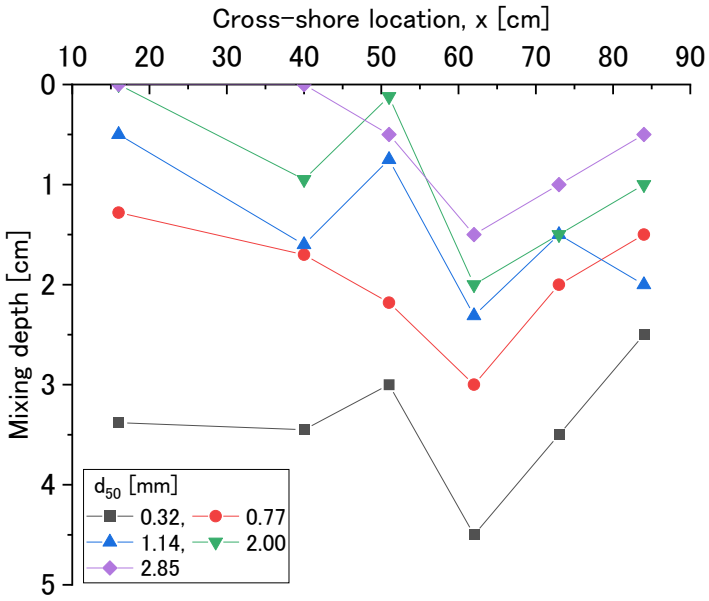

Figure 8. Spatial distributions of mixing depth for different sediment diameters in the surf zone.

Table 3. Summary of mixing depth at each location.

Case	d_{50} [mm]	Mixing depth, z_m [cm]						
		x [cm]						Ave.
		16	40	50	62	73	80	
1	0.32	3.38	3.45	3.00	4.50	3.50	2.50	3.39
2	0.77	1.28	1.70	2.18	3.00	2.00	1.50	1.94
3	1.14	0.50	1.60	0.75	2.31	1.50	2.00	1.44
4	2.00	0.00	0.95	0.12	2.00	1.50	1.00	0.93
5	2.85	0.00	0.00	0.50	1.50	1.00	0.50	0.58

3.3 Fluid motion in the surf zone

The velocity fields in the surf zone were calculated using the LES model. Figure 9

shows the flow velocity vectors calculated in a cross-shore vertical section at the middle of the flume (y = 12 cm). These velocity maps indicate that the wave propagation is towards the shore, and wave breaking occurred approximately at x = 50 cm, and the impingement point is between x = 60-65 cm. Furthermore, the water surface rises after the wave breaking occurs, i.e., at approximately x = 70 cm, and re- impingement occurs at x = 80 cm. These calculation results were consistent with the observed experimental results. The complex flow field generated by wave breaking appears to be well represented by the model in a qualitative manner.

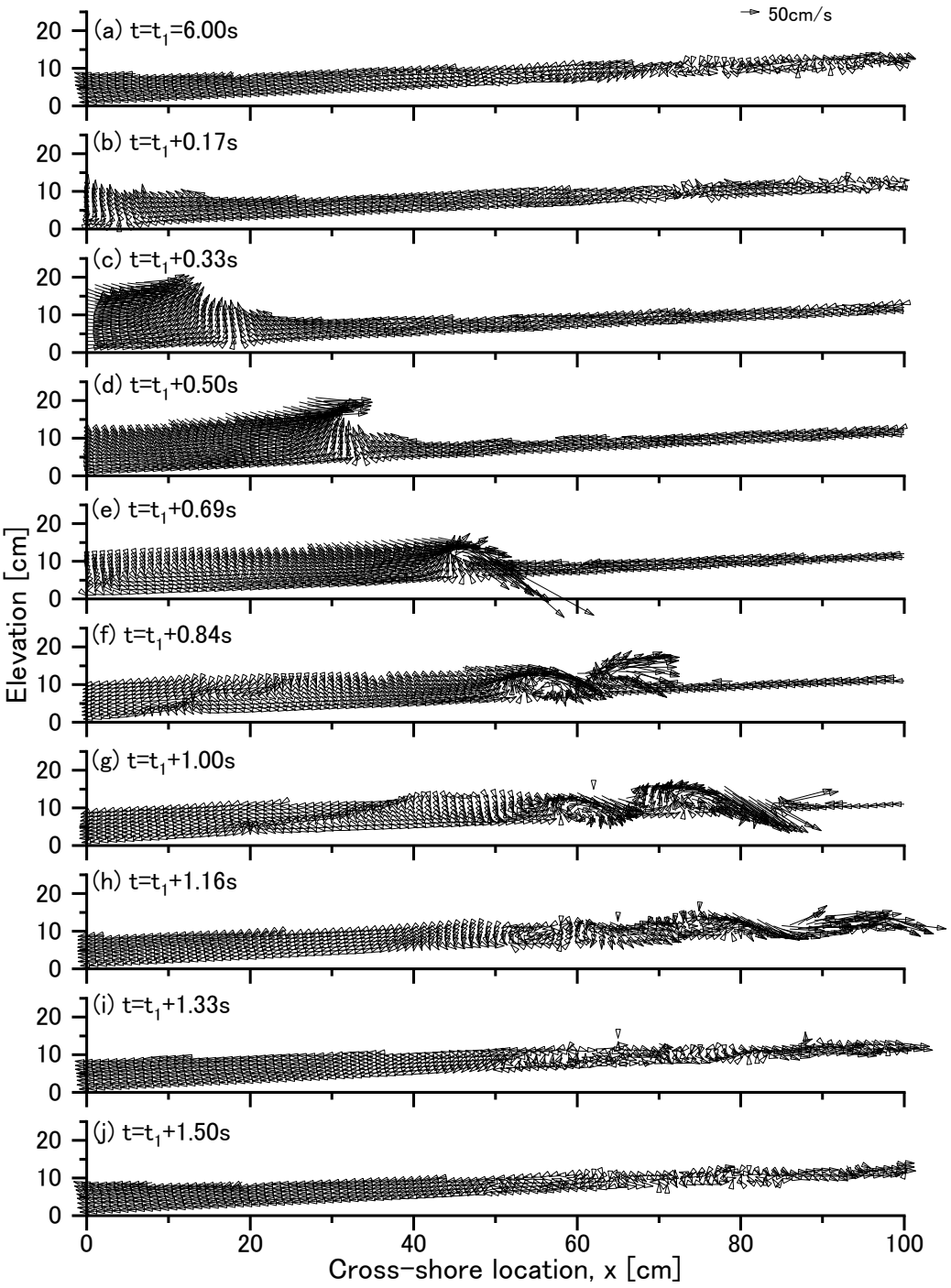

333

334 Figure 9. Velocity vectors in a cross-shore vertical section at the middle of the flume (*y*

335 = 12 cm) using LES model.

336

4. Discussion

4.1 Comparison between vertical velocity and mixing depth

In the surf zone, sediment mixing occurred due to the water flow and velocity generated by waves and wave breaking phenomena. In this section, the correlation between mixing depth and flow velocity is determined using the LES model results.

Figure 10 shows the spatial distribution of ensemble-averaged vertical velocity calculated using four waves in the bottom grid cells of the selected domain. The spatial distributions of the observed mixing depth were superimposed on the right vertical axis. In case of vertical velocity, the thin black solid and dashed lines indicate the downward, w_-, and upward, w_+, vertical velocities, respectively, and the thick line indicates the root mean square vertical velocity, i.e., $w_{rms} = \sqrt{(w_+^2 + w_-^2)/2}$. From the velocity distribution curves and the mixing depth, both values are larger at around the impinging point, x = 62 cm. Although some discrepancies exist, the trends of the spatial distribution are similar between vertical velocity and mixing depth of each sediment diameter.

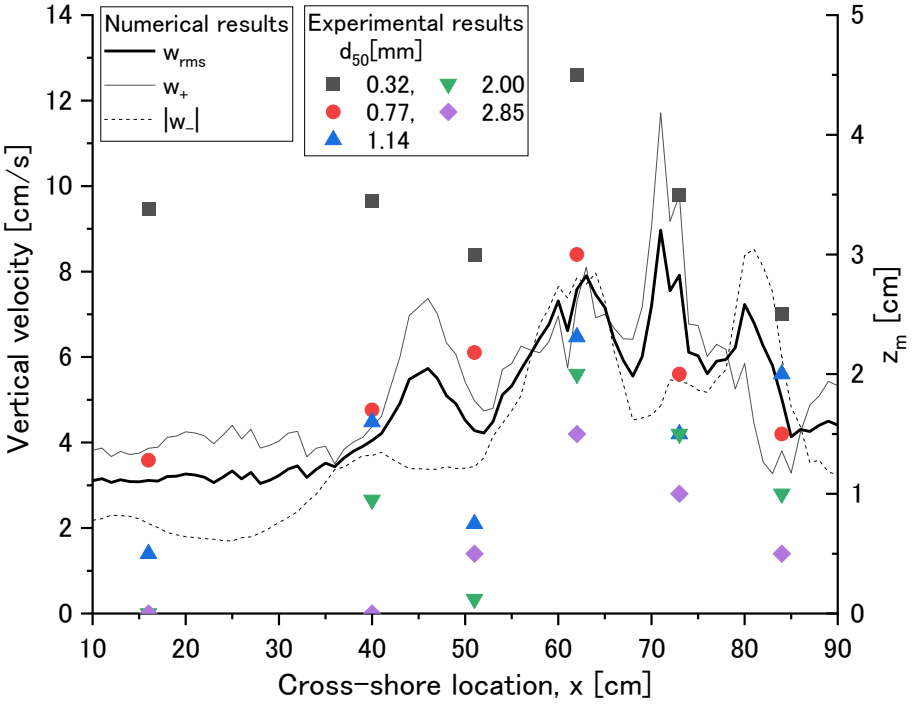

353

354 Figure 10. Spatial distribution of averaged vertical velocity and mixing depth for

355 various sediment diameters. Each line indicates the numerical model outputs, and the

356 symbols indicate the experimental results.

357

358

359 ***4.2 Estimation of mixing depth using vertical velocity***

360 In order to estimate the mixing depth of each sediment diameter using the RMS vertical

361 velocity, the velocity was normalized by falling velocity (Julien, 2002):

362 $$w_f = \frac{8\nu}{d}\left(\sqrt{1+\frac{sgd^3}{72\nu^2}}-1\right) \quad (3)$$

363 where ν is the dynamic viscosity of the fluid, s is the specific density of the sediment

364 in the water, and d is the average sediment diameter.

365 Figure 11 shows the relation between normalized vertical velocity that
366 calculated by the LES, $w^* = w_{rms} / w_f$, and observed mixing depths in the experiments
367 for all cases. It is noted that when the vertical velocity increases the mixing depth also
368 increases. For each sediment diameter, a smaller diameter causes a larger mixing depth.
369 Each color of the dashed line indicates the location of the core sampling. The peak of
370 the mixing occurred at the impingement point for all cases, x = 62 cm. In the offshore
371 region, relatively larger mixing occurs compared to the depth in the onshore region.
372 Moreover, the spatial distribution of the mixing depth is the same as expected, and a
373 smaller diameter has a larger mixing depth.
374 Overall, in spite of the difference in sediment diameters and cross-shore
375 location, the mixing depth could be expressed in the following mathematical
376 relationship:
377 $$z_m = 1.75 \ln(w^*) + 2.45 \quad (4)$$
378 The correlation coefficient, R was 0.92.
379

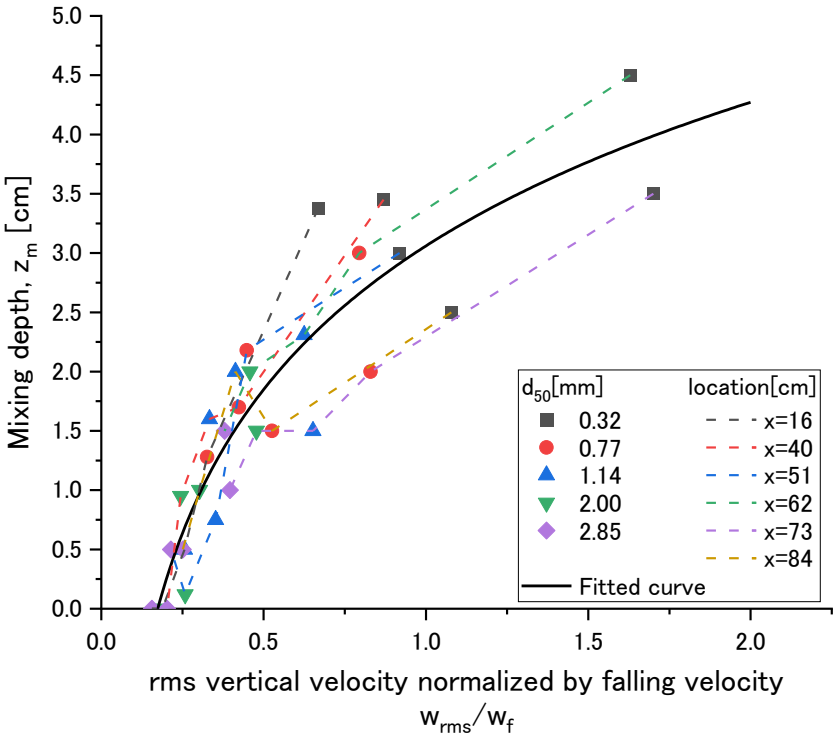

Figure 11. Correlation between normalized vertical velocity calculated by the LES and observed mixing depths in the experiments for different sediment diameters.

The correlation between measured and calculated mixing depth for all cases are shown in Figure 12. The solid line indicates the line of best-fit between laboratory experiments and simulations, whereas a dotted line indicates the 1:1 line correlation between two parameters. Although the smaller diameter of the sand, i.e., 0.32 and 0.77 mm, vary compared to large sediment diameters, despite the sediment diameter difference, calculated mixing depths show good agreement.

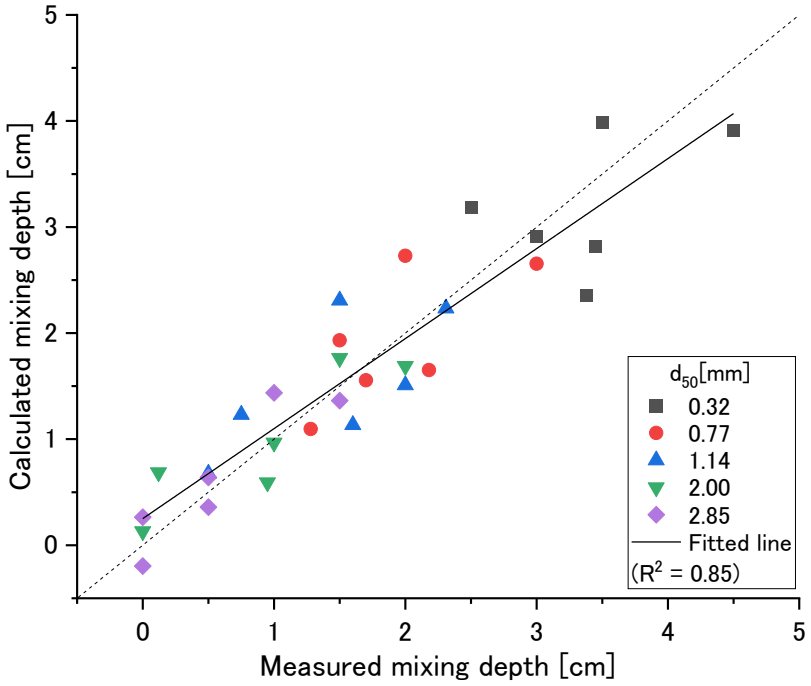

Figure 12. Measured and calculated values of normalized mixing depth

5. Conclusions

Laboratory experiments were conducted to investigate the spatial distribution of sediment mixing depth in the surf zone for five different sediment diameters. In experiments, sediment diameters of d_{50} = 0.32, 0.77, 1.14, 2.0 and 2.85 mm were used, and the same diameters of fluorescent sand tracers were sprinkled on the water surface to determine the mixing depth. After a pre-defined period of regular wave generation, core sampling was taken at six cross-shore locations in the surf zone and analyzed for mixing depth characteristics.

The results revealed that the vertical mixing occurred at all cross-shore locations with spatial variations. The trend of the spatial distribution for each diameter

406 was similar though the maximum mixing depth occurred at the impinging point, and the
407 depths decreased for both onshore and offshore wards. However, larger mixing depth
408 was given by the smaller grain size, i.e., 0.32 mm, and the mixing depth decreased
409 logarithmically when the diameter increased. Moreover, the flow velocity field in the
410 surf zone was determined using a Large Eddy Simulation (LES) model and discussed
411 the relationship between spatial distribution of sediment mixing depth and the vertical
412 flow velocities on the bed. The spatial distribution of mixing depth has a correlation
413 with RMS vertical velocities regardless of the sediment diameter. The proposed vertical
414 mixing depth equation could estimate the correct depth with better accuracy.
415 As a further study, combining laboratory and numerical results with field
416 observations needs to be investigated in order to further verify the applicability of the
417 proposed new mathematical model (Eq. 4) and established a correlation for spatial
418 distribution of vertical sediment mixing depth in the field.
419
420 **Acknowledgements**
421 The authors would like to thank Professor Yoshiyuki Nakamura and Dr Hiroto Higa of
422 Yokohama National University for providing fruitful comments and suggestions to
423 improve the manuscript. This research study was partially funded by the Great Britain
424 Sasakawa Foundation (GBSF) grant no. 5696.
425
426 **References**
427 Aagaard, T., & Jensen, S. G. (2013). Sediment concentration and vertical mixing under
428 breaking waves. *Marine Geology,* Elsevier, 336, 146-159.
429 doi.org/10.1016/j.margeo.2012.11.015

Anfuso, G., Gracia, F. J., Andrés, J., Sánchez, F., Del Río, L., & López-Aguayo, F. (2000). Depth of disturbance in mesotidal beaches during a single tidal cycle. *Journal of Coastal Research,* Coastal Education & Research Foundation, 446-457. https://www.jstor.org/stable/4300053

Bellido, C., Anfuso, G., Plomaritis, T. A., & Rangel-Buitrago, N. (2011). Morphodynamic behaviour, disturbance depth and longshore transport at Camposoto Beach (Cadiz, SW Spain). *Journal of Coastal Research*, Coastal Education & Research Foundation, SI 64, 35-39. https://www.jstor.org/stable/26482128

Botton, M. L., Loveland, R. E., & Jacobsen, T. R. (1988). Beach erosion and geochemical factors: influence on spawning success of horseshoe crabs (Limulus polyphemus) in Delaware Bay. *Marine Biology*, Springer, 99(3), 325-332. doi.org/10.1007/BF02112124

Christensen, E. D., & Deigaard, R. (2001). Large eddy simulation of breaking waves. *Coastal Engineering*, 42(1), 53-86. doi.org/10.1016/S0378-3839(00)00049-1

Ciavola, P., Taborda, R., & Ferreira, Ó. (1997a). Field observations of sand-mixing depths on steep beaches. *Marine Geology,* Elsevier, 141(1-4), 147-156. doi.org/10.1016/S0025-3227(97)00054-6

Ciavola, P., Taborda, R., Ferreira, O., & Dias, J. A. (1997b). Field measurements of longshore sand transport and control processes on a steep meso-tidal beach in Portugal. *Journal of Coastal Research*, 1119-1129. https://www.jstor.org/stable/4298720

Dolphin, T. J., Hume, T. M., & Parnell, K. E. (1995). Oceanographic processes and sediment mixing on a sand flat in an enclosed sea, Manukau Harbour, New Zealand. *Marine Geology*, Elsevier, 128(3-4), 169-181. doi.org/10.1016/0025-

3227(95)00097-I

Ferreira, O., Ciavola, P., Taborda, R., Bairros, M., & Dias, J. A. (2000). Sediment mixing depth determination for steep and gentle foreshores. *Journal of Coastal Research,* Coastal Education & Research Foundation, 830-839. https://www.jstor.org/stable/4300093

Fucella, J. E., & Dolan, R. (1996). Magnitude of subaerial beach disturbance during northeast storms. *Journal of Coastal Research*, Coastal Education & Research Foundation, 420-429. https://www.jstor.org/stable/4298494

Gaughan, M. K. (1978). Depth of disturbance of sand in surf zones. *16th International Conference on Coastal Engineering,* ASCE, 1513-1530. doi.org/10.1061/9780872621909.091

Greenwood, B., & Hale, P. B. (1980). Depth of activity, sediment flux, and morphological change in a barred nearshore environment. *In The coastline of Canada* (vol. 80, 89-109). Halifax: Geological Survey of Canada.

Gunaratna, T., Akimoto, S., & Suzuki, T. (2018). Laboratory experiments of sediment mixing and the effect of bottom eddies. *Journal of Japan Society of Civil Engineers,* Ser. B3 (Ocean Engineering), 74(2), I_737-I_742. doi.org/10.2208/jscejoe.74.I_737

Jackson, D. W. T., & Malvarez, G. (2002). A new, high-resolution 'depth of disturbance' instrument (SAM) for use in the surf zone. *Journal of Coastal Research*, Coastal Education & Research Foundation, (36 (10036)), 406-413. doi.org/10.2112/1551-5036-36.sp1.406

Jackson, N. L., & Nordstrom, K. F. (1993). Depth of activation of sediment by plunging breakers on a steep sand beach. *Marine Geology,* Elsevier, 115(1-2), 143-151. doi.org/10.1016/0025-3227(93)90079-B

Julien, P. Y. (2002). *River Mechanics.* Cambridge University Press, UK, 434p.

Katoh, K., & Tanaka, N. (1986). Local movements of sand in the surf zone. *20th International Conference on Coastal Engineering,* ASCE, 1240-1254. doi.org/10.1061/9780872626003.091

King, C. A. M. (1951). Depth of disturbance of sand on sea beaches by waves. *Journal of Sedimentary Research,* Society of Sedimentary Geology, 21(3), 131-140. doi.org/10.1306/D4269445-2B26-11D7-8648000102C1865D

Kraeuter, J. N., & Fegley, S. R. (1994). Vertical disturbance of sediments by horseshoe crabs (Limulus polyphemus) during their spawning season. *Estuaries,* Springer, 17(1), 288-294. doi.org/10.2307/1352578

Kraus, N. C., & Smith, J. M. (1994). SUPERTANK Laboratory Data Collection Project. Volume 1. Main Text (No. CERC-94-3). *Coastal Engineering Research Center (CERC),* Vicksburg, USA. https://apps.dtic.mil/sti/citations/ADA275975

Kraus, N. C. (1985). Field experiments on vertical mixing of sand in the surf zone. *Journal of Sedimentary Research*, 55(1), 3-14. doi.org/10.1306/212F85E9-2B24-11D7-8648000102C1865D

Owens, E. H., & Lee, K. (2003). Interaction of oil and mineral fines on shorelines: review and assessment. *Marine Pollution Bulletin*, Elsevier, 47(9-12), 397-405. doi.org/10.1016/S0025-326X(03)00209-1

Roselli, R. A. R., Vernengo, G., Brizzolara, S., & Guercio, R. (2019). SPH simulation of periodic wave breaking in the surf zone-A detailed fluid dynamic validation. *Ocean Engineering,* Elsevier, 176, 20-30. doi.org/10.1016/j.oceaneng.2019.02.013

Saini, S., Jackson, N. L., & Nordstrom, K. F. (2009). Depth of activation on a mixed sediment beach. *Coastal Engineering,* Elsevier, 56(7), 788-791.

502 doi.org/10.1016/j.coastaleng.2009.02.002
503 Sherman, D. J., Short, A. D., & Takeda, I. (1993). Sediment mixing-depth and bedform
504 migration in rip channels. *Journal of Coastal Research,* Coastal Education &
505 Research Foundation, 39-48. https://www.jstor.org/stable/25735722
506 Sherman, D. J., Nordstrom, K. F., Jackson, N. L., & Allen, J. R. (1994). Sediment
507 mixing-depths on a low-energy reflective beach. *Journal of Coastal Research,*
508 Coastal Education & Research Foundation, 297-305.
509 https://www.jstor.org/stable/4298217
510 Silva, A., Taborda, R., Rodrigues, A., Duarte, J., & Cascalho, J. (2007). Longshore drift
511 estimation using fluorescent tracers: new insights from an experiment at Comporta
512 Beach, Portugal. *Marine Geology,* Elsevier, 240(1-4), 137-150.
513 doi.org/10.1016/j.margeo.2007.02.009
514 Smagorinsky, J. (1963). General circulation experiments with the primitive equations: I.
515 The basic experiment. *Monthly Weather Review,* 91(3), 99-164.
516 doi.org/10.1175/1520-0493(1963)091<0099:GCEWTP>2.3.CO;2
517 Sunamura, T., & Kraus, N. C. (1984). Prediction of average mixing depth of sediment in
518 the surf zone. *Marine Geology,* Elsevier, 62(1-2), 1-12. doi.org/10.1016/0025-
519 3227(84)90051-3
520 Suzuki, T., Inami, Y., Yanagishima, S., Sakihama, S., & Cox, D. T. (2019). Sediment
521 particle movements observed using tracers under accretive wave conditions in the
522 nearshore zone. *Coastal Engineering Journal,* JSCE, 61(4), 472-485.
523 doi.org/10.1080/21664250.2019.1629863
524 Suzuki, T., Okayasu, A., & Shibayama, T. (2007). A numerical study of intermittent
525 sediment concentration under breaking waves in the surf zone. *Coastal Engineering,*

526 Elsevier, 54(5), 433-444. doi.org/10.1016/j.coastaleng.2006.11.002
527 Vila-Concejo, A., Harris, D. L., Power, H. E., Shannon, A. M., & Webster, J. M. (2014).
528 Sediment transport and mixing depth on a coral reef sand apron. *Geomorphology,*
529 Elsevier, 222, 143-150. doi.org/10.1016/j.geomorph.2013.09.034
530 Watanabe, Y., & Saeki, H. (1999). Three-dimensional large eddy simulation of breaking
531 waves. *Coastal Engineering Journal,* JSCE, 41(3-4), 281-301.
532 doi.org/10.1142/S0578563499000176
533 Williams, A. T. (1971). An analysis of some factors involved in the depth of disturbance
534 of beach sand by waves. *Marine Geology,* Elsevier, 11(3), 145-158.
535 doi.org/10.1016/0025-3227(71)90003-X
536 Zhou, Z., Hsu, T. J., Cox, D., & Liu, X. (2017). Large-eddy simulation of wave-
537 breaking induced turbulent coherent structures and suspended sediment transport on
538 a barred beach. *Journal of Geophysical Research: Oceans*, 122(1), 207-235.
539 doi.org/10.1002/2016JC011884
540 Zou, S., & Dalrymple, R. A. (2006). Sediment suspension simulation under oscillatory
541 flow by SPH-SPS method. *30th International Conference on Coastal Engineering,*
542 ASCE, 2477-2484. doi.org/10.1142/9789812709554_0209
543